Int. J. Electrochem. Sci., 7 **(2012)** 6191 - 6201

International Journal of
ELECTROCHEMICAL
SCIENCE
www.electrochemsci.org

Nanoparticles-Assembly of $LiMn_2O_4$ Hollow Microspheres with Improved Rate Capability and Cycleability for Lithium Ion Batteries

C. Y. Sun[1], *H. Y. Yang*[2], *J. Xie*[1], *G. S. Cao*[1], *X. B. Zhao*[1], *T. J. Zhu*[1,*]

[1] State Key Laboratory of Silicon Materials and Department of Materials Science and Engineering, Zhejiang University, Hangzhou 310027, China
[2] Pillar of Engineering Product Development, Singapore University of Technology and Design 20 Dover Drive Singapore, 138682, Singapore
[*]E-mail: zhutj@zju.edu.cn

Received: 23 May 2012 / *Accepted:* 4 June 2012 / *Published:* 1 July 2012

In this paper, we demonstrate the synthesis and application of spinel $LiMn_2O_4$ with unique micro-/nano-hybrid structure as a promising cathode for high power Li-ion batteries. $LiMn_2O_4$ with high crystallinity has been prepared successfully by solid-state lithiation of hexagonal MnO_2 via a template-engaged reaction. The product presents hollow microsphere with ultrathin outer shell assembled by nanoparticles. Electrochemical measurements indicate that $LiMn_2O_4$ hollow microspheres exhibit superior rate capability and cycleability to the solid microspheres and commercial bulk counterparts. The initial discharge capacity of 91 mAh g^{-1} can be delivered at 20 C, and capacity retention of over 90% is obtained after 500 cycles at this high rate. The superior electrochemical performance is attributed to the unique micro-/nano-hybrid structure that facilitates the fast Li-intercalation kinetics and good structure stability.

Keywords: self-template reaction; micro/nano-hybrid structure; Li-ion batteries， cathode materials

1. INTRODUCTION

Li-ion batteries have attracted enormous attention due to their potential applications in high-power devices, such as electric vehicles and hybrid electric vehicles [1-3]. Although having gained success in portable devices, commercial Li-ion batteries often fail to fulfill the requirements of high power density and long cycle life [4]. Hence, the development of cathode material that can suffer high power and long cycling is a fundamental issue for further application. Among various cathodes, spinel $LiMn_2O_4$ is a promising candidate because of its low-cost, high abundance, environmental friendliness

and better safety [1, 5]. However, bulk $LiMn_2O_4$ from conventional solid-state combustion often suffers from low capacity and poor cycling under large current density due to severe polarization that is usually resulted from long Li-ion diffusion distance in the bulk [6-9]. To date, various approaches have been widely investigated to enhance high-rate performance. The design and synthesis of nanometer-sized materials have been verified to be an excellent solution because of their large surface area that can enhance the contact between active materials and electrolyte [10-13].

Recently, hollow spherical structure has attracted considerable attention due to its particular structure that facilitates the penetration of the electrolyte and buffers the volume expansion/contraction upon repeated cycling [14, 15]. Han et al. [16] has reported hollow microspheres of SnO_2 with high initial capacity and superior cycling stability. Hollow microspheres of CuO reported by Wang and co-workers [17] displayed specific capacity of over 600 mAh g^{-1} during up to 50 cycles. Si hollow nanospheres also exhibited improved cycle life and rate capacity [18]. Recently, $LiMn_2O_4$ micro-/nano-spheres have also been verified to be excellent spinel-based electrodes [19, 20].

In view of the particular advantages of hollow microspheres, synthesis and testing of $LiMn_2O_4$ hollow microspheres can be challenging but very attractive. In this work, we have succeeded in designing and synthesis of unique hollow microspheres of $LiMn_2O_4$ (HS-LMO) with nanoparticles-assembled ultrathin shell by a self-support template. The electrochemical tests demonstrate that the as-obtained HS-LMO exhibits high initial capacity and durable high-rate capability.

2. EXPERIMENTAL

All the reagents were analytical grade and used without further purification. $MnCO_3$ microspheres were prepared by the precipitation method reported [21] with modification. In a typical experiment, 100 ml of ethanol was added to the $MnSO_4$ solution (500 mL, 0.01 M) with stirring to form a homogeneous solution. Then, NH_4HCO_3 solution (500 mL, 0.1 M,) was slowly dropped into the mixed solution under stirring. After the reaction, the white precipitate was collected, washed with distilled water and ethanol repeatedly and dried at 50 °C under vacuum for 12 h. The obtained $MnCO_3$ microspheres serve as original template and manganese source for producing hollow microspheres of $LiMn_2O_4$ (HS-LMO). The detail is as follows: first, $MnCO_3$ microspheres were pre-calcined at 300 °C for 12 h to form hierarchical $MnCO_3$@MnO_2-shell/$MnCO_3$-core; then, hollow microspheres of MnO_2 (HS-MO) were obtained by dissolving $MnCO_3$ with 0.1 M HCl; finally, HS-LMO was prepared by calcining HS-MO with LiOH at 700 °C for 10 h in air. For comparison, electrochemical properties of other two kinds of $LiMn_2O_4$ were characterized. One was solid microsphere of $LiMn_2O_4$ (SS-LMO) that was also prepared by same solid-state reactions using the prepared $MnCO_3$ microsphere and LiOH as precursors. The other was commercial $LiMn_2O_4$ from Aldrich (C-LMO).

The crystalline structure of the products was identified by X-ray diffraction (XRD) on a Rigaku D/Max-2550pc powder diffractometer equipped with Cu K_α radiation (λ = 1.5406 Å). The morphologies of the products were observed by field emission scanning electron microscopy (SEM, Hitachi S4800), transmission electron microscopy (TEM, Philips FEI 200 CX) and high-resolution transmission electron microscope (HRTEM, JEOL 2100F). The chemical composition of the product

was determined by inductively coupled plasma-atomic emission spectrometry (ICP-AES, IRIS Intrepid II XSP). Fourier transform infrared spectrum (FTIR) of the materials was carried out by a Bruker Tensor 27 spectrometer using KBr pellet technique.

The electrochemical properties of the materials were evaluated by using CR2025-type coin cells with lithium metal as the negative electrode. The cathode slurry was made by mixing active material, acetylene black and polyvinylidene fluoride (PVDF) in a weight ratio of 80: 10: 10 in N-methyl pyrrolidone (NMP) with magnetic stirring. The blended slurry was cast onto Al foil current collector and dried at 80 °C under vacuum for 12 h followed by pressing at 10 MPa. The cells were assembled in an argon-filled glove box. The electrolyte was 1 M $LiPF_6$ in ethylene carbonate (EC)-dimethyl carbonate (DMC) (1:1 in volume). Polypropylene micro-porous film (Celgard 2300) was used as the separator. Galvanostatic charging/discharging measurements were performed in the voltage range of 3.5-4.3 V *vs.* Li/Li^+ at various current densities using a BTS battery tester (Neware, Shenzhen, China). Cycle voltammorgams (CVs) measurements were conducted on a CHI 660C electrochemistry workstation (Chenhua instrument Co, Shanghai, China) at a scan rate of 0.1 mV s^{-1}.

3. RESULTS AND DISCUSSION

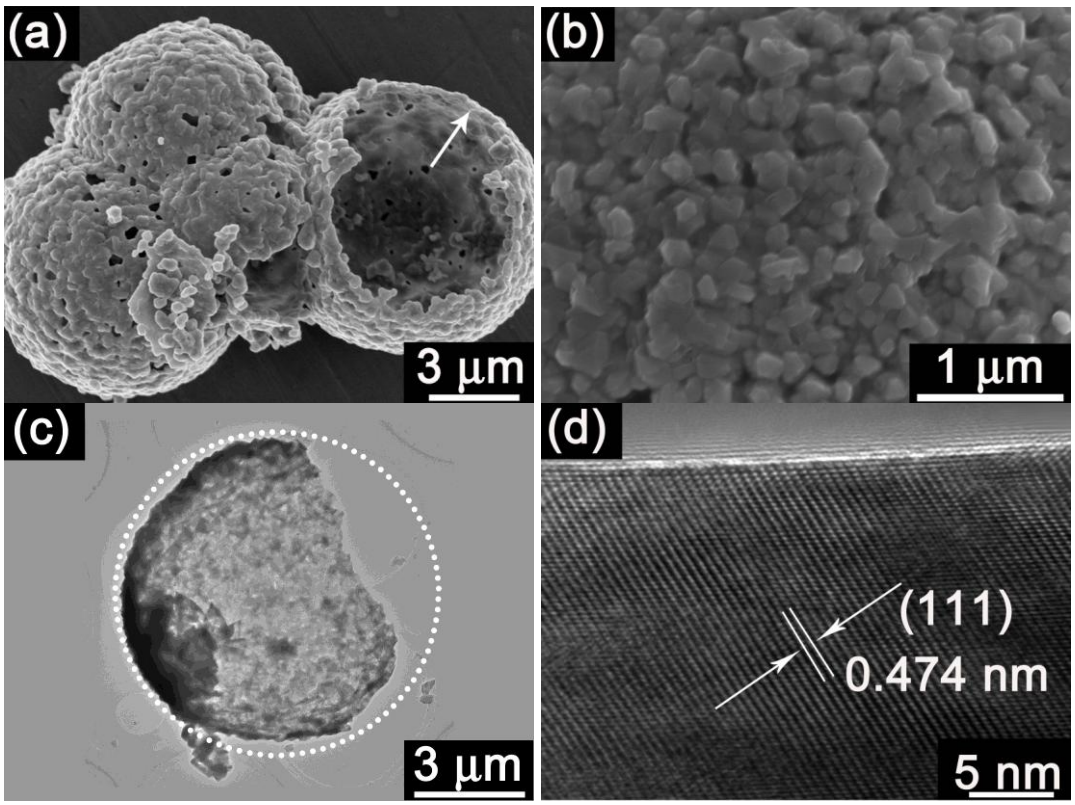

Figure 1. Morphology of HS-LMO: (a) low magnification SEM image, (b) SEM image for the surface of a microsphere, (c) TEM image of a broken microsphere, and (d) HRTEM image of a nanoparticle on the shell.

Fig. 1 displays the typical morphologies of $LiMn_2O_4$ formed via template-engaged reaction, using hollow microspheres of MnO_2 served as the direct self-sacrifice template. Fig. 1a shows $LiMn_2O_4$ hollow microspheres with a diameter of about 9 □m. We can also observe ultrathin shell with the thickness of about 200 nm (2% of the diameter of microspheres). Outer shell is assembled by close-packed nanoparticles with a diameter of about 100 nm (Fig. 1b), which is different from smooth surface of $LiMn_2O_4$ hollow microsphere reported [19]. Typical TEM image also confirms hollow structure and ultrathin shell of the product (Fig. 1c). HRTEM image focused on a nanoparticle (Fig. 1d) shows the crystalline character of the as-synthesized compound. The measured interplanar distance of 0.474 nm is consistent well with that of (111) plane of cubic spinel $LiMn_2O_4$, revealing high crystallinity of as-obtained HS-LMO.

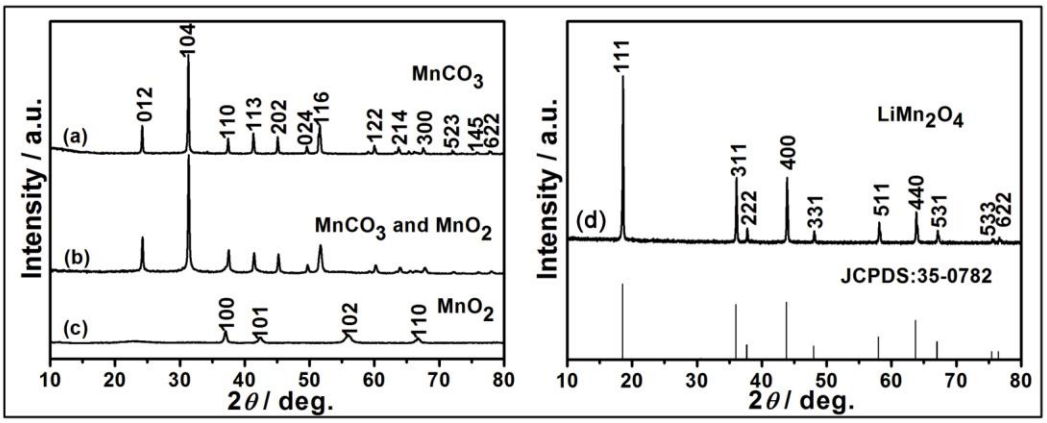

Figure 2. XRD patterns of (a) $MnCO_3$ microspheres, (b) hierarchical structure ($MnCO_3$@MnO_2-shell/$MnCO_3$-core) obtained after pre-calcining $MnCO_3$ at 300 °C for 12 h, (c) MnO_2 obtained after removal of $MnCO_3$ using 0.1 M HCl and (d) $LiMn_2O_4$ obtained after template-engaged lithiation process.

HS-LMO was formed by lithiation of hexagonal MnO_2 with the prepared $MnCO_3$ served as manganese source and original template. The detail of transformation among phases is investigated by XRD patterns (Fig. 2). From Fig. 2a, the XRD pattern of the initial product by the precipitation method can be indexed to single phase $MnCO_3$ (*R-3c*, JCPDS No. 44-1472). After pre-calcination at 300 °C for 12 h, the $MnCO_3$ phase is still maintained and MnO_2 phase is not detected (Fig. 2b). But after dissolving $MnCO_3$ by 0.1 M HCl, the diffraction peaks of hexagonal-symmetrical MnO_2 are observed clearly, such as (100), (101), (102), (110), which are consistent with JCPDS No. 30-0820 (Fig. 2c). From Fig. 2b and 2c, it is suggested that rhombohedral $MnCO_3$ is partially converted into hexagonal MnO_2 and the mixture of $MnCO_3$@MnO_2 is formed. Besides, compare with invisible diffraction peaks of MnO_2, diffraction peaks of $MnCO_3$ are shown clearly, which can support that $MnCO_3$ is the dominating phase in mixture after pre-calcination. It may be due to low content of MnO_2 in mixture that results in its invisibility. It may also be attributed to particular hierarchical structure ($MnCO_3$@MnO_2) that MnO_2 is not detected before removal of $MnCO_3$ outer layer (Fig. 2b). In Fig. 2d, after solid-state lithiation reaction of MnO_2 at high temperature, the product is identified as cubic

spinel $LiMn_2O_4$ with a space group of *Fd3m* (JCPDS No. 35-0782). The composition of the synthesized compound was further investigated by inductively coupled plasma-atomic emission spectrometry (ICP-AES) method. The result shows atomic ratio of Li/Mn is 0.52, indicating forming a lithium-rich spinel compound.

Herein, HS-LMO was prepared by a facile template-engaged reaction as illustrated in Fig. 3a, different from the synthesis of $LiMn_2O_4$ nanospheres by low-temperature chemical lithiation reaction using LiI as lithium source in previous report [20]. Formation of HS-LMO can be mainly attributed to hierarchical structure of $MnCO_3$ microspheres, suitable pre-calcination condition, removal of $MnCO_3$ by HCl and subsequent high-temperature lithiation reaction. The uniform $MnCO_3$ microspheres with a diameter of about 9 □m were formed during the precipitation reaction as seen in Fig. 3b. The surface of the microsphere consists of nanopyramids (the inset in Fig. 3b).

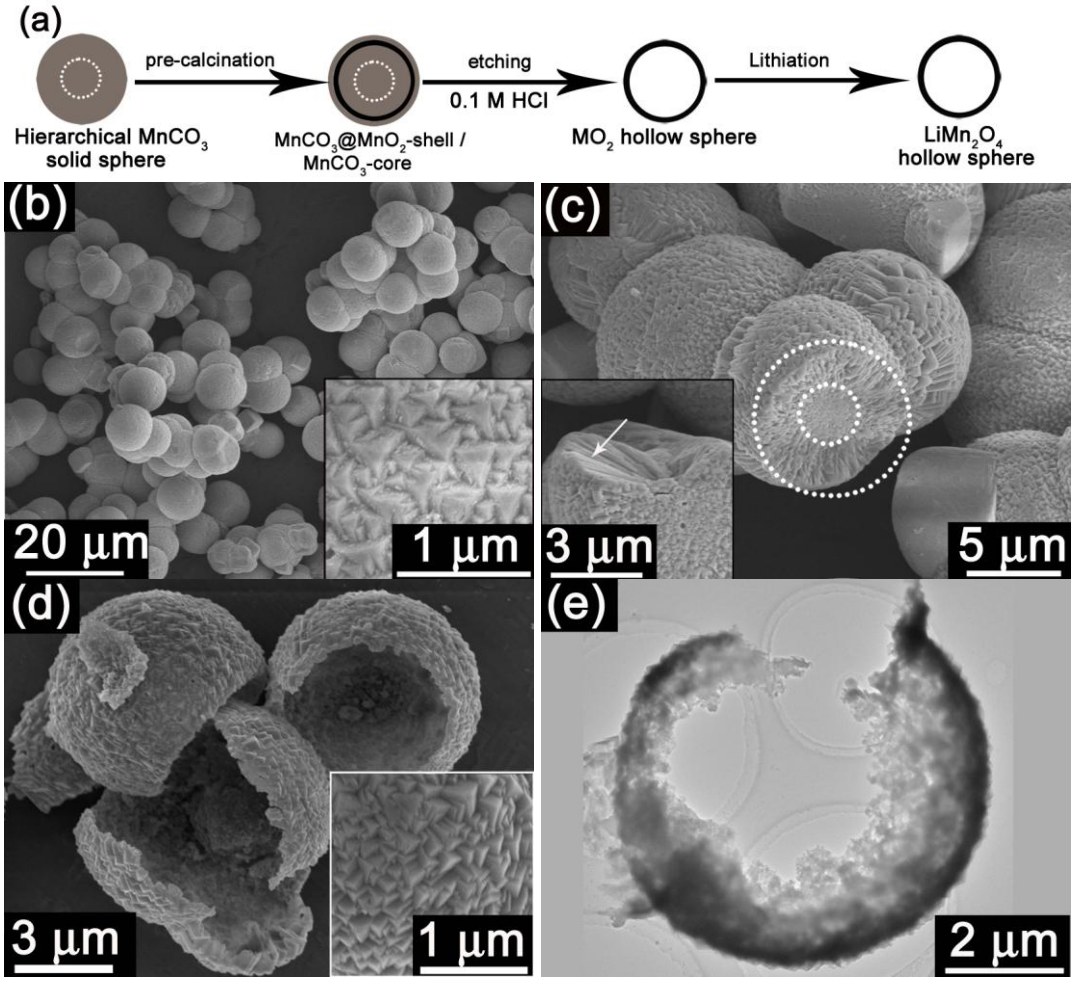

Figure 3. (a) Schematic illustration of the formation of HS-LMO, SEM images of (b) $MnCO_3$ microspheres prepared by the precipitation method, the inset shows the outer surface of a microsphere, (c) a cross-sectional view of $MnCO_3$ microsphere, the inset shows image of further broken microsphere, and (d) HS-MO obtained after removing $MnCO_3$ with 0.1 M HCl, the inset shows the surface of outer shell of HS-MO, (e) TEM image of a broken HS-MO.

From the crossed-sectional view of a broken $MnCO_3$ microsphere (Fig. 3c), different structures between inner core and outer shell can be observed as marked by inner and outer dotted circles, contributing to hierarchical $MnCO_3$@MnO_2-shell/$MnCO_3$-core after pre-calcination of $MnCO_3$ microspheres [22]. Upon pre-calcination, the surface of $MnCO_3$ shell was oxidized to MnO_2 in advance and processed from outer layer to inner layer due to more contact with air, contributing to formation of $MnCO_3$@MnO_2 shell [14, 22, 23]. In this case, only oxidation layer of MnO_2 was formed on the surface because $MnCO_3$ could only be partially decomposed or under-calcined at this low temperature, whereas inner core still kept as the $MnCO_3$ salt [23]. Thus, hierarchical structure ($MnCO_3$-core/$MnCO_3$@MnO_2-shell) is formed, which is beneficial for further tailoring into a hollow structure due to favour solubility of $MnCO_3$ in diluted acid and difficult dissolution of MnO_2. After 0.1 M HCl was employed to remove $MnCO_3$ from the hierarchical strcture ($MnCO_3$@MnO_2-shell/$MnCO_3$-core), hollow spherical MnO_2 was obtained and pyramid-like structure was well-preserved on the surface of microspheres (Fig. 3d). Hollow structure can be further supported by TEM image (Fig. 3e). Ultrathin shell is formed because of low content of MnO_2 shell in the mixture (Fig. 3d and 3e). After calcinated with LiOH at 700 °C, HS-MO was converted to HS-LMO with well-preserved hollow spherical structure despite of formating some pores within the shell (Fig. 1). In addition, the morphology of outer shell converted from nanopyramids to nanoparticles as seen from Fig. 1b and 3d. The smooth dense shell was converted to nanoparticles-packed spherical shell with some nanopores, which could facilitate the penetration of electrolyte.

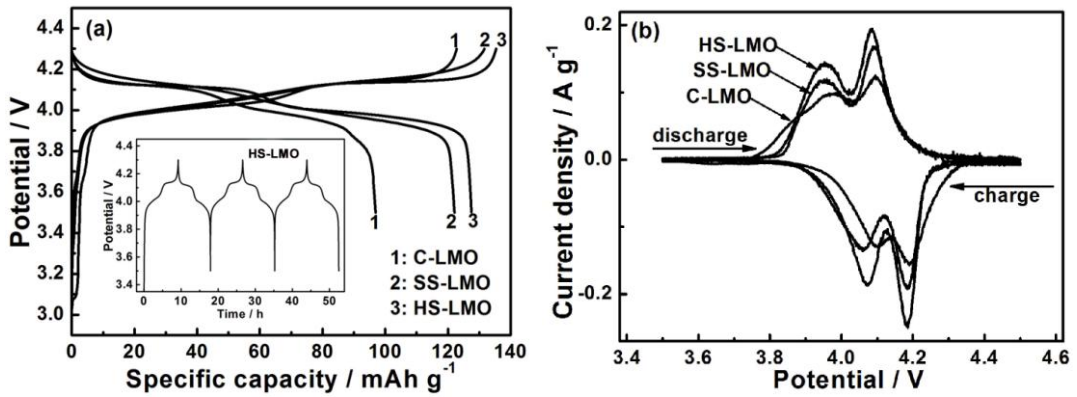

Figure 4. (a) The first charge/discharge voltage profiles of $LiMn_2O_4$/Li cells at 0.1 C between 3.5 and 4.3 V, the inset shows charge/discharge profiles of the HS-LMO/Li cell during first three cycles, and (b) CV plots between 3.5 and 4.5 V with a scan rate of 0.1 mV s^{-1}.

Coin-type cells were assembled to evaluate the electrochemical behaviors of all three samples. Fig. 4a displays the first charge/discharge curves of three electrodes at 0.1 C (1 C = 148 mA g^{-1}). The first discharge capacity of HS-LMO electrode is about 127 mAh g^{-1}, higher than that of another two electrodes (122 mAh g^{-1} for SS-LMO and 97 mAh g^{-1} for C-LMO). Furthermore, HS-LMO electrode displays high initial coulombic efficiency (~93%), suggesting less Li-consuming surface reactions during the first charging/discharging cycle [12]. In the successive cycling, HS-LMO/Li cell took nearly same time during charging/discharging (the inset in Fig. 4a), demonstrating that the cells supply

coulombic efficiency of nearly 100%. Two pronounced charge/discharge plateaus can be observed for all three samples, demonstrating Li^+ ions extraction/interaction reactions. Cycle voltammorgams were performed for three samples to further investigate potentials of Li-insertion/extraction. Two pairs of separated redox peaks can be clearly observed, which are associated with the potential plateaus in the charge/discharge curves, suggesting that Li^+ ions are extracted or inserted from/into the spinel matrix with a two-step mechanism [24]. Among three samples, HS-LMO exhibits sharper and higher-symmetrical redox peaks than both C-LMO and SS-LMO, revealing higher crystallinity of HS-LMO and better interface with the electrolyte.

To further investigate potential application in high power devices, the cells are discharged at various rates ranging from 1 to 20 C after charging at 1 C rate (Fig. 5a). Discharge capacities of all the samples gradually decrease with improving discharge rate, indicating the diffusion-controlled kinetics process for electrode reaction [11]. Obvious difference can be observed easily among three cathodes, HS-LMO shows a lower fading rate than another two samples. In addition, the discharge capacity of HS-LMO can be recovered when current decreased from 20 to 1 C, indicating good reversibility of this cathode that may facilitate Li^+ ions insertion/deinsertion into/from spinel matrix. Using 1 C charging rate, discharge profiles of HS-LMO/Li cell are shown in Fig. 5b. The average potential and discharge capacity decrease gradually with the improving discharge rate. At the same time, two discharge potential plateaus become sloped gradually, which may be due to electrode overpotentials and increased internal ohmic (*IR*) drop at high rates [10]. But HS-LMO electrode still displays discharge capacity of 91 mAh g^{-1} at 20 C rate. The superior rate capability of HS-LMO can be attributed to their structure features. Spinel $LiMn_2O_4$ has a three-dimensional lithium diffusion path due to favorable crystal, resulting in easier lithium exchanging between active materials and electrode. It is also ascribed to nanoparticles which are beneficial for faster Li-insertion.

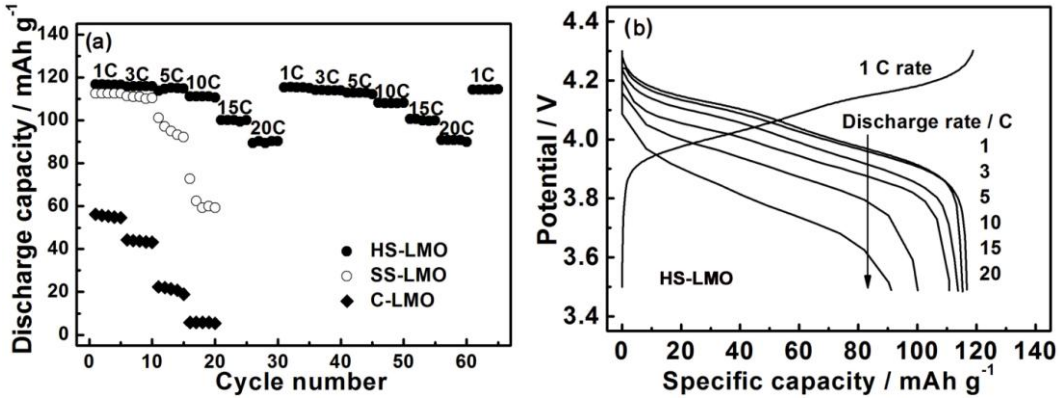

Figure 5. (a) Discharge capacity with cycle number under varied discharge rates after charging at 1 C, and (b) discharge voltage profiles at different current rates for HS-LMO.

High-rate behaviors of all the materials are further investigated to identify potential applications of three electrodes for high-power devices. Three materials are discharged at 10 C after charging at 1 C rate (Fig. 6a). Remarkably, HS-LMO displays the average discharge capacity of over

110 mAh g^{-1}, while another two materials fail to sustain high-rate requirement with much lower discharge capacity during 100 cycles.

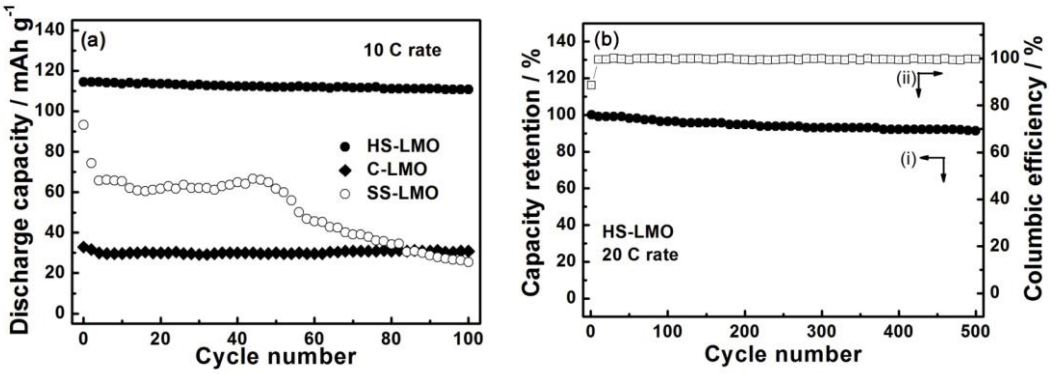

Figure 6. (a) Comparison of discharge capacity among C-LMO, SS-LMO and HS-LMO at 10 C, and (b) discharge capacity retention and coulombic efficiency plots of HS-LMO/Li cell as a function of cycle number at 20 C.

To fully evaluate high-rate cycleability, HS-LMO based cells are discharged at higher rate (20 C) and conditions up to 500 cycles were performed using 1 C charge rate. As shown in Fig. 6b, the discharge capacity retention of HS-LMO/Li cell can still maintain over 90% after 500 cycles and coulombic efficiency can still maintain nearly 100% except the first cycle, displaying superior high-rate cycleability. This may be due to their special micro-/nano-hybrid structure: hollow structure with some nanopores facilitates the penetration of the electrolyte, which maximizes the contact of active material with electrolyte; outer shell can accommodate strain from the volume changes upon Li^+ ions insertion/extraction, which is beneficial for sustaining structure stability during long cycling; nanoparticles on the shell can shorten Li^+ ions diffusion distance and facilitate rapid Li^+ ions diffusion, which can decrease polarization during charging/discharging under large current, leading to superior high-rate cycleability.

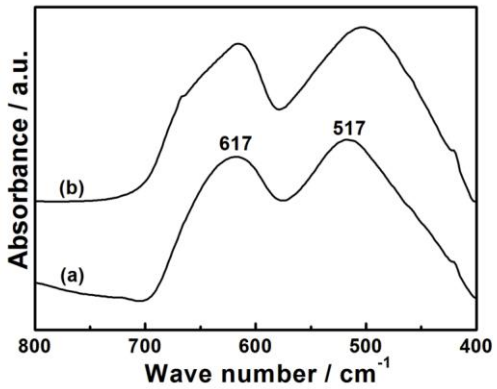

Figure 7. (a) Transmission FTIR spectra of HS-LMO electrodes: (a) as-assembled before initial charging-discharging and (b) after 200 cycles with discharging of 10 C rate.

Compare with hollow spherical $LiMn_2O_4$ prepared in the previous reports [19, 20], hollow microspheres in this work exhibit higher capacity and better cycling stability. Discharge capacity of 91 mAh g^{-1} can be delivered under the current density of 2.96 A g^{-1}, much higher than another two hollow microspheres [19, 20]. This is due to special preparation method in our work, without K^+ cations involved during preparation and higher crystallinity from high-temperature calcination [25]. The presence of K^+ cations may impede the diffusion of Li^+ ions, resulting in a low capacity and inferior cycle life [26]. Besides, it is commonly considered that samples with high crystallinity usually display higher capacity and better cycling stability [27].

Structural stability of HS-LMO electrode was investigated after prolonged cycling under high-rate current. Spinel structure (AB_2O_4) can be investigated by FTIR spectra (Fig. 7). Before charging/discharging, the FTIR spectra of HS-LMO displays two separated peaks (617 cm^{-1} and 517 cm^{-1}), corresponding to the vibrations of tetrahedral LiO_4 and octahedral MnO_6 [28, 29]. After 200 cycles with discharging at 10 C, the FTIR characteristic is kept almost unchanged except a slight shift towards to lower frequencies. The slight shift and broadness of the peak located at 517 cm^{-1} may be due to the formation of lithium-poor spinel compound [28].

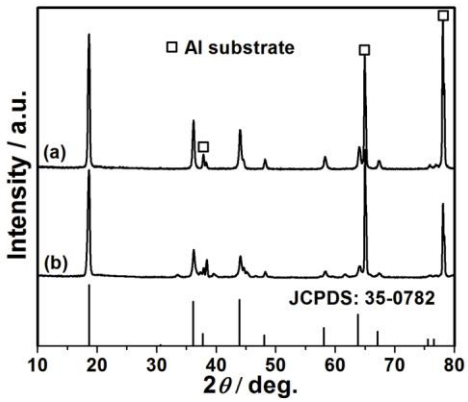

Figure 8. (a) XRD patterns of HS-LMO electrode after cycled for (a) 100 times and (b) 200 times with discharging at 10 C, the asterisk denotes aluminum substrate.

From Fig. 8, XRD patterns can also support that HS-LMO electrode still keeps cubic spinel structure and no possible impurity of Mn_2O_3 presents after cycling at high rate, displaying excellent structure stability during fast Li-intercalation.

4. CONCLUSIONS

In summary, we succeeded in designing and synthesizing spinel $LiMn_2O_4$ with micro-/nano-hybrid structure by a facile self-template method. The prepared $LiMn_2O_4$ presents hollow microspheres with nanoparticles-assembled ultrathin shell. In this approach, the morphology of self-support MnO_2 template could be well-preserved after high-temperature calcination. The synthesized $LiMn_2O_4$ hollow microspheres were verified to bear good crystallinity, and spinel matrix could be well-preserved after

long cycling under high-rate current. As cathodes for Li-ion batteries, they display superior rate capability and cycling stability, which is attributed to their special micro-/nano-hybrid structure and high crystallinity. Considering durable high-rate capability and facile fabrication method, nanoparticles-assembled hollow microspheres of $LiMn_2O_4$ can serve as a promising cathode for high-power Li-ion batteries.

ACKNOWLEDGEMENT
The authors would like to acknowledge financial support from the National Natural Science Foundation of China (No. 51101139), the Qianjiang Talents Project of Science Technology Department of Zhejiang Province (2011R10021), the Ph.D. Programs Foundation of Ministry of Education of China (No. 20100101120024), and the Foundation of Education Department of Zhejiang Province (No. Y201016484). HYY thanks financial support from SUTD-ZJU/RES/042011 grant.

References

1. A. S. Arico, P. Bruce, B. Scrosati, J. M. Tarascon, W. van Schalkwijk, *Nat. Mater*. 4 (2005) 366-377.
2. S. Y. Chung, J. T. Bloking, Y. M. Chiang, *Nat. Mater*. 1 (2002) 123-128.
3. P. L. Taberna,; S. Mitra,; P. Poizot,; P. Simon,; J. M. Tarascon, *Nat. Mater*. 5 (2006) 567-573.
4. H. Li, Z. Wang, L. Chen, X. Huang, *Adv. Mater*. 21 (2009) 4593-4607.
5. P. Bruce, B. Scrosati, J. M. Tarascon, *Angew. Chem., Int. Edit*. 47 (2008) 2930-2946.
6. S. Lim, J. Cho, *Electrochem. Commun*. 10 (2008) 1478-1481.
7. M. M. Thackeray, *J. Electrochem. Soc*. 142 (1995) 2558-2563.
8. Y. Wang, G. Cao, *Adv. Mater*. 20 (2008) 2251-2269.
9. Y. G. Guo, Y. S. Hu, W. Sigle, J. Maier, *Adv. Mater*. 19 (2007) 2087-2091.
10. H. W. Lee, P. Muralidharan, R. Ruffo, C. M. Mari, Y. Cui, D. K. Kim, *Nano Lett*. 10 (2010) 3852-3856.
11. Y. L. Ding, J. Xie, G. S. Cao, T. J. Zhu, H. M. Yu, X. B. Zhao, *Adv. Funct. Mater*. 21 (2011) 348-355.
12. Y. G. Guo, J. S. Hu, L. J. Wan, *Adv. Mater*. 20 (2008) 2878-2887.
13. F. Cheng, H. Wang, Z. Zhu, Y. Wang, T. Zhang, Z. Tao, J. Chen, *Energy Environ. Sci*. 4 (2011) 3668-3675.
14. Y. L. Ding, X. B. Zhao, J. Xie, G. S. Cao, T. J. Zhu, H. M. Yu, C. Y. Sun, *J. Mater. Chem*. 21 (2011) 9475-9479.
15. A. M. Cao, J. S. Hu, H. P. Liang, L. J. Wan, *Angew. Chem., Int. Edit*. 44 (2005) 4391-4395.
16. S. Han, B. Jang, T. Kim, S. M. Oh, T. Hyeon, *Adv. Funct. Mater.* 15 (2005) 1845-1850.
17. S. Q. Wang, J. Y. Zhang, C. H. Chen, *Scripta Mater*. 57 (2007) 337-340.
18. H. Ma, F. Cheng, J. Y. Chen, J. Z. Zhao, C. S. Li, Z. L. Tao, J. Liang, *Adv. Mater*. 19 (2007) 4067-4070.
19. X. Xiao, J.; Lu, Y. Li, *Nano Res*. 3 (2010) 733-737.
20. J. Luo, L. Cheng, Y. Xia, *Electrochem. Commun*. 9 (2007) 1404-1409.
21. J. Fei, Y. Cui, X. Yan, W. Qi, Y. Yang, K. Wang, Q. He, J. Li, *Adv. Mater*. 20 (2008) 452-456.
22. J. Cao, Y. Zhu, L. Shi, L. Zhu, K. Bao, S. Liu, Y. Qian, *Eur. J. Inorg. Chem*. 2010, 1172-1176.
23. L. Wang, F. Tang, K. Ozawa, Z. G. Chen, A. Mukherj, Y. Zhu, J. Zou, H. M. Cheng, G. Q. Lu, *Angew. Chem., Inter. Edit.* 48 (2009) 7048-7051.
24. Y. Xia, M. Yoshio, *J. Electrochem. Soc*. 143 (1996) 825-833.
25. K. Kanamura, K. Dokko, T. Kaizawa, *J. Electrochem. Soc*. 152 (2005) A391-A395.

26. J. Y. Luo, H. M. Xiong, Y. Y. Xia, *J. Phys. Chem. C*. 112 (2008) 12051-12057.
27. E. Hosono, T. Kudo, I. Honma, H. Matsuda, H. Zhou, *Nano Lett.* 9 (2009) 1045.
28. T. J. Richardson, S. J. Wen, K. A. Strichel, P. N. Ross Jr, E. J. Cairns, *Mater. Res. Bull*. 32 (1997) 609-618.
29. P. Kalyani, N. Kalaiselvi, N. Muniyandi, *J. Power Sources* 111 (2002) 232-238.